

Event-by-Event Direction Reconstruction of Solar Neutrinos in a High Light-Yield Liquid Scintillator

A. Allega,¹ M. R. Anderson,¹ S. Andringa,² J. Antunes,^{2,3} M. Askins,^{4,5} D. J. Auty,⁶ A. Bacon,⁷ J. Baker,^{8,9} N. Barros,^{2,10} F. Barão,^{2,3} R. Bayes,^{9,1} E. W. Beier,⁷ T. S. Bezerra,¹¹ A. Bialek,^{8,9} S. D. Biller,¹² E. Blucher,¹³ E. Caden,^{8,9} E. J. Callaghan,^{4,5} M. Chen,¹ S. Cheng,¹ B. Cleveland,^{8,9} D. Cookman,¹² J. Corning,¹ M. A. Cox,^{14,2} R. Dehghani,¹ J. Deloye,⁹ M. M. Depatie,^{9,1} F. Di Lodovico,¹⁵ J. Dittmer,¹⁶ K. H. Dixon,¹⁵ E. Falk,¹¹ N. Fatemighomi,⁸ R. Ford,^{8,9} A. Gaur,⁶ O. I. González-Reina,¹⁷ D. Gooding,¹⁸ C. Grant,¹⁸ J. Grove,¹ S. Hall,⁸ A. L. Hallin,⁶ W. J. Heintzelman,⁷ R. L. Helmer,¹⁹ C. Hewitt,¹² B. Hreljac,¹ V. Howard,⁹ J. Hu,⁶ R. Hunt-Stokes,¹² S. M. A. Hussain,^{1,8} A. S. Inácio,^{12,2,20} C. J. Jillings,^{8,9} S. Kaluzienski,¹ T. Kaptanoglu,^{4,5} P. Khaghani,⁹ H. Khan,⁹ J. R. Klein,⁷ L. L. Kormos,²¹ B. Krar,¹ C. Kraus,^{9,8} C. B. Krauss,⁶ T. Kroupová,⁷ C. Lake,⁹ L. Lebanowski,^{4,5} J. Lee,¹ C. Lefebvre,¹ Y. H. Lin,¹ V. Lozza,^{2,20} M. Luo,⁷ A. Maio,^{2,20} S. Manecki,^{8,1,9} J. Maneira,^{2,20} R. D. Martin,¹ N. McCauley,¹⁴ A. B. McDonald,¹ C. Mills,¹¹ G. Milton,¹² I. Morton-Blake,¹² M. Mubasher,⁶ A. Molina Colina,^{9,8} D. Morris,¹ S. Naugle,⁷ L. J. Nolan,²² H. M. O’Keeffe,²¹ G. D. Orebi Gann,^{4,5} J. Page,¹¹ K. Paleshi,⁹ W. Parker,¹² J. Paton,¹² S. J. M. Peeters,¹¹ L. Pickard,^{4,5,23} P. Ravi,⁹ A. Reichold,¹² S. Riccetto,¹ M. Rigan,¹¹ J. Rose,¹⁴ R. Rosero,²⁴ J. Rumleskie,⁹ I. Semeneč,¹ P. Skensved,¹ M. Smiley,^{4,5} J. Smith,^{8,9} R. Svoboda,²³ B. Tam,^{12,1} J. Tseng,¹² S. Valder,¹¹ E. Vázquez-Jáuregui,¹⁷ C. J. Virtue,⁹ J. Wang,¹² M. Ward,¹ J. R. Wilson,¹⁵ J. D. Wilson,⁶ A. Wright,¹ J. P. Yanez,⁶ S. Yang,⁶ M. Yeh,²⁴ Z. Ye,⁷ S. Yu,^{1,9} Y. Zhang,^{25,26} K. Zuber,¹⁶ and A. Zummo⁷

(The SNO+ Collaboration)

¹Queen’s University, Department of Physics, Engineering Physics & Astronomy, Kingston, ON K7L 3N6, Canada

²Laboratório de Instrumentação e Física Experimental de Partículas (LIP),
Av. Prof. Gama Pinto, 2, 1649-003, Lisboa, Portugal

³Universidade de Lisboa, Instituto Superior Técnico (IST),
Departamento de Física, Av. Rovisco Pais, 1049-001 Lisboa, Portugal

⁴University of California, Berkeley, Department of Physics, CA 94720, Berkeley, USA

⁵Lawrence Berkeley National Laboratory, 1 Cyclotron Road, Berkeley, CA 94720-8153, USA

⁶University of Alberta, Department of Physics, 4-181 CCIS, Edmonton, AB T6G 2E1, Canada

⁷University of Pennsylvania, Department of Physics & Astronomy,
209 South 33rd Street, Philadelphia, PA 19104-6396, USA

⁸SNOLAB, Creighton Mine #9, 1039 Regional Road 24, Sudbury, ON P3Y 1N2, Canada

⁹Laurentian University, School of Natural Sciences,
935 Ramsey Lake Road, Sudbury, ON P3E 2C6, Canada

¹⁰Universidade de Coimbra, Departamento de Física (FCUC), 3004-516, Coimbra, Portugal

¹¹University of Sussex, Physics & Astronomy, Pevensey II, Falmer, Brighton, BN1 9QH, UK

¹²University of Oxford, The Denys Wilkinson Building, Keble Road, Oxford, OX1 3RH, UK

¹³The Enrico Fermi Institute and Department of Physics,
The University of Chicago, Chicago, IL 60637, USA

¹⁴University of Liverpool, Department of Physics, Liverpool, L69 3BX, UK

¹⁵King’s College London, Department of Physics,
Strand Building, Strand, London, WC2R 2LS, UK

¹⁶Technische Universität Dresden, Institut für Kern und Teilchenphysik, Zellescher Weg 19, Dresden, 01069, Germany

¹⁷Universidad Nacional Autónoma de México (UNAM),

Instituto de Física, Apartado Postal 20-364, México D.F., 01000, México

¹⁸Boston University, Department of Physics, 590 Commonwealth Avenue, Boston, MA 02215, USA

¹⁹TRIUMF, 4004 Wesbrook Mall, Vancouver, BC V6T 2A3, Canada

²⁰Universidade de Lisboa, Faculdade de Ciências (FCUL),
Departamento de Física, Campo Grande, Edifício C8, 1749-016 Lisboa, Portugal

²¹Lancaster University, Physics Department, Lancaster, LA1 4YB, UK

²²Queen Mary, University of London, School of Physics and Astronomy, 327 Mile End Road, London, E1 4NS, UK

²³University of California, Davis, 1 Shields Avenue, Davis, CA 95616, USA

²⁴Brookhaven National Laboratory, Chemistry Department,
Building 555, P.O. Box 5000, Upton, NY 11973-500, USA

²⁵Research Center for Particle Science and Technology,
Institute of Frontier and Interdisciplinary Science,

Shandong University, Qingdao 266237, Shandong, China

²⁶Key Laboratory of Particle Physics and Particle Irradiation of Ministry of Education,
Shandong University, Qingdao 266237, Shandong, China

The direction of individual ^8B solar neutrinos has been reconstructed using the SNO+ liquid scintillator detector. Prompt, directional Cherenkov light was separated from the slower, isotropic scintillation light using time information, and a maximum likelihood method was used to reconstruct the direction of individual scattered electrons. A clear directional signal was observed, correlated with the solar angle. The observation was aided by a period of low primary fluor concentration that resulted in a slower scintillator decay time. This is the first time that event-by-event direction reconstruction in high light-yield liquid scintillator has been demonstrated in a large-scale detector.

I. INTRODUCTION

Organic liquid scintillator (LS) detectors play a central role in particle physics, particularly in studies of neutrinos, where numerous breakthrough measurements have been made in areas such as solar neutrinos [1], reactor antineutrinos [2–5] and neutrinoless double beta decay [6]. Several large scale LS detectors are currently in operation [7–9] with more under construction [10] or being planned [11, 12].

There has been much interest in recent years in enhancing the capabilities of such detectors by separating Cherenkov light from the scintillation signal so as to provide directional information while maintaining the energy resolution of high light-yield scintillators [13–25]. Several recent community-planning exercises in both the U.S. and Europe have highlighted the importance of these developments [26–29]. This concept is central to several small-scale demonstrators both under construction and in operation [30–32], as well as large-scale experiments currently under development [11, 12]. Detectors have used Cherenkov light before in low-light yield scintillators, such as Liquid Scintillator Neutrino Detector (LSND), which had an isotropic to Cherenkov light ratio of 5:1 [33] and MiniBooNE, which had a ratio of 3:1 [34, 35]. However, the Cherenkov component in high light-yield LS detectors typically only represents a few percent of the overall light signal, posing a considerably greater challenge. In addition to having a different wavelength profile, the prompt and directional nature of this light offers potential handles to distinguish it from the slower, isotropic scintillation signal. This can be aided by further slowing the characteristic scintillation time either by introducing primary fluors with longer intrinsic time constants [13, 36] or by reducing the primary fluor concentration to reduce the nonradiative coupling with the solvent [15, 16].

During its commissioning phase, the SNO+ experiment operated with an initial concentration of 0.6 g/L 2,5-diphenyloxazole (PPO) in the linear alkylbenzene (LAB) solvent, resulting in a scintillation decay timescale of >10 ns. Data during this time period shows a clear directional signal from ^8B solar neutrino interactions. While a recent study by the Borexino Collaboration [37, 38] found a correlation with the solar direction for individual early Cherenkov photons from a few percent of their solar events, and used those integrated distributions in fits to help extract signals, this is the first time that a

large-scale experiment has demonstrated event-by-event direction reconstruction in high light-yield liquid scintillator.

II. THE SNO+ DETECTOR AND DATA SELECTION

SNO+ is a multipurpose neutrino detector located 2 km underground at SNOLAB in Ontario, Canada. Much of the infrastructure has been repurposed from the SNO experiment, including 9362 photomultiplier tubes (PMTs) and a 6 m radius acrylic vessel (AV). Significant upgrades have been made to the detector, allowing for the AV to be filled with LS [39]. Further details of the SNO+ detector can be found in [9].

In order to select a pure sample of ^8B solar neutrinos for the current study, an energy region for the scattered electron of approximately 5–15 MeV was used [40]. This removes the vast majority of events due to Uranium and Thorium chain (U/Th) chain backgrounds as well as events associated with muons. The higher energy events in this sample are expected to provide better directional information, compared to those below 5 MeV, due to the increased number of Cherenkov photons, reduced electron multiple scattering and neutrino interaction kinematics. A dead time of 20 s was also enforced after any energy deposition above 15 MeV in order to remove any further activity following muon events. A fiducial radius of 5.5 m from the center of the AV was used to select events from a region of more uniform detector optical response. After cuts, the only expected background events result from atmospheric neutrinos and the decays of ^{208}Tl and ^{210}Tl , which results in a total of ~ 1 expected events within the dataset.

III. DATASETS

During the period of April – October 2020 (Period 1, exposure 23 kt d), SNO+ was partially filled with scintillator that floated on a larger volume of water inside the AV. The LS portion comprised 365 t with a PPO concentration of 0.6 g/L. The interface with the water region was ~ 75 cm above the AV equator. *In situ* measurements of light emitted from low energy background events in the LS region during this phase indicated a yield of ~ 300 detected photoelectrons per MeV of deposited electron

energy. A parametrization of the inherent scintillator timing profile was derived based on a comparison of data with simulations for ^{214}Bi background events, tagged via the associated alpha decay of ^{214}Po , and has the following form:

$$P(t) = \sum_{i=1}^3 A_i \frac{e^{-t/\tau_i} - e^{-t/\tau_r}}{\tau_i - \tau_r} \quad (1)$$

where P is the probability of photon emission, t is the time of emission, A_i is the fraction of light in the i th component, τ_i is the fall time of the i th component and τ_r is the common rise time, found to be 0.8 ns. This parameterization is shown in Fig. 1 and the derived constants are given in Table I.

i	1	2	3
τ_i (ns)	13.5	23	98.5
A_i	0.55	0.335	0.115

TABLE I: The derived scintillation timing profile parameters of LAB with 0.6 g/L PPO.

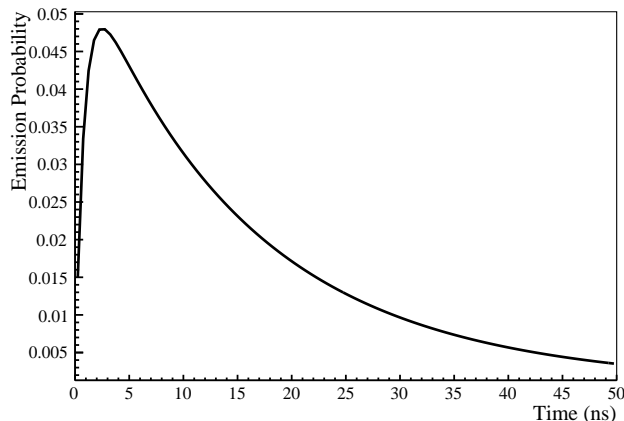


FIG. 1: Parameterized time profile of scintillation light emission for electrons in LAB with 0.6 g/L PPO based on comparisons of ^{214}Bi background events in data and simulations.

For the Period 1 dataset, an extra fiducial volume constraint was implemented in order to avoid proximity to the scintillator-water interface, where optical effects became nonuniform. Events were excluded which reconstructed within the water volume, and within 25 cm above the interface. From this dataset, 20 solar neutrino candidates were extracted.

Between April and June 2021 (Period 2, exposure 15 kt d) the detector was filled with 780 t of LS at 0.6 g/L PPO concentration. The scintillator optical, timing and light-yield characteristics were confirmed to be unchanged from Period 1. Seventeen solar neutrino candidates were extracted from this period, which were then combined with Period 1 to create a single dataset.

The total dataset had an exposure of 38 kt d and 37 selected events, which is statistically consistent with the expectation of 40 events, derived from the flux presented in [41].

IV. CHERENKOV SEPARATION IN SNO+

Reconstruction of event direction relies on isolating the instantaneous Cherenkov light from the scintillation signal using timing information. A “time residual” is defined as:

$$t_{\text{res}} = t_{\text{hit}} - t_{\text{event}} - t_{\text{flight}} \quad (2)$$

where t_{hit} is the recorded hit time of the PMT, t_{event} is the reconstructed event time and t_{flight} is the estimated time of flight of the photon, assuming a straight line light path. The latter two terms result from a maximum likelihood fit to an assumed pointlike vertex position based on timing information from all hit PMTs in the event. The distribution of t_{res} is largely dominated by the inherent time spectrum of scintillation/Cherenkov light, the PMT time response, and uncertainties in the reconstructed vertex position. Within the selected energy range, the 3D vertex resolution is 24–26 cm. The anisotropy in the early light due to the Cherenkov component can be identified by using this timing information in conjunction with the parameter θ_γ , defined as the angle between the estimated photon direction (*i.e.* from the reconstructed vertex to the hit PMT) and the initial direction of the original electron, as shown in Fig. 2a.

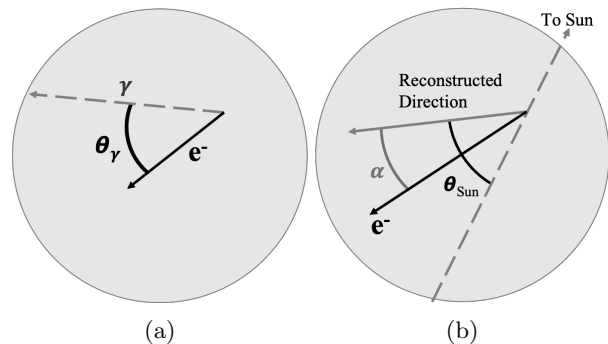


FIG. 2: Definitions of angles referenced in this paper: θ_γ is the angle between the electron’s travel direction and the photon direction; α is the angle between the true and reconstructed direction of the electron; and θ_{Sun} is the angle between the reconstructed event direction and the solar direction (assumed true direction of the neutrino).

It is possible to clearly see this anisotropy in the $\cos \theta_\gamma$ distribution on the rising edge of the scintillator timing profile in simulations of 6 MeV electrons using measured scintillation characteristics, where 6 MeV was chosen to represent a typical electron recoil energy from a ^8B solar neutrino for this dataset. A clear Cherenkov peak can

be seen in Fig. 3 at low t_{res} near the expected emission angle of $\cos \theta_\gamma = 0.66$. There is also a slight bias in the “backwards” direction (towards $\cos \theta_\gamma = -1$) evident in the plot. This is due to bias in the vertex reconstruction caused by the earlier Cherenkov photons “pulling” the best fit vertex along the direction of motion. This effect was also noted in Borexino’s directionality studies [37, 38]. This suggests that it might be possible to improve reconstruction by simultaneously fitting for both vertex and direction. While this is currently under study, the present analysis treats these two aspects separately.

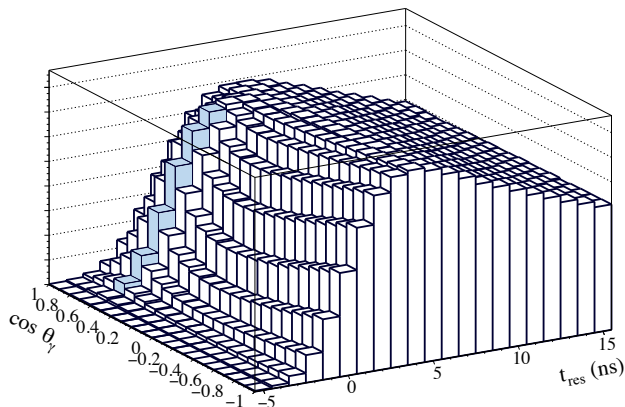


FIG. 3: Distribution of photon hits in $\cos \theta_\gamma$ and t_{res} for simulated 6 MeV electrons in LAB with a PPO concentration of 0.6 g/L. A clear peak can be seen at low t_{res} near the expected Cherenkov angle, $\cos \theta_\gamma = 0.66$, highlighted in blue.

V. DIRECTION RECONSTRUCTION

The distribution in Fig. 3 is used as a probability density function (PDF) for a maximum likelihood reconstruction of event direction. Results of this direction reconstruction for electrons of different energies simulated in the SNO+ detector are shown in Fig. 4, where α is defined as the angle between the true direction and the reconstructed direction as shown in Fig. 2b. Table II shows simulation predictions for the percentage of events with $\cos \alpha > 0.8$ for different electron energies.

As shown in Fig. 4, higher energy electrons yield better direction reconstruction owing to increased photon sampling as well as a reduced impact from electron multiple scattering. Increased effective photocathode coverage and/or slower scintillator formulations should be able to extend the usable range of direction reconstruction to lower energies [25].

The impact of multiple scattering and vertex reconstruction bias on the direction fit are illustrated in Fig. 5 for simulated 6 MeV electrons. From this investigation, it is clear the features near $\cos \alpha = 0$ and $\cos \alpha = -1$ are caused by vertex reconstruction effects.

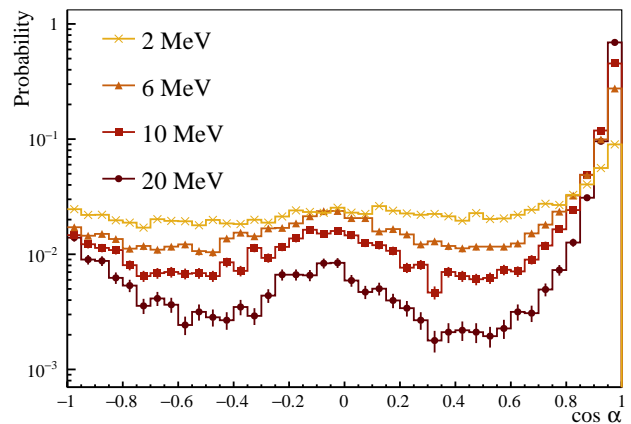


FIG. 4: Results of direction reconstruction of simulated electrons of different energies, with error bars displaying statistical uncertainties.

Electron Energy (MeV)	% with $\cos \alpha > 0.8$
2	21.9 ± 0.4
6	45.6 ± 0.6
10	64.6 ± 0.7
20	83.0 ± 0.8

TABLE II: Energy dependence of direction reconstruction for electrons simulated in the SNO+ detector, with statistical uncertainties. The performance is quantified by the percentage of events that reconstruct with $\cos \alpha > 0.8$.

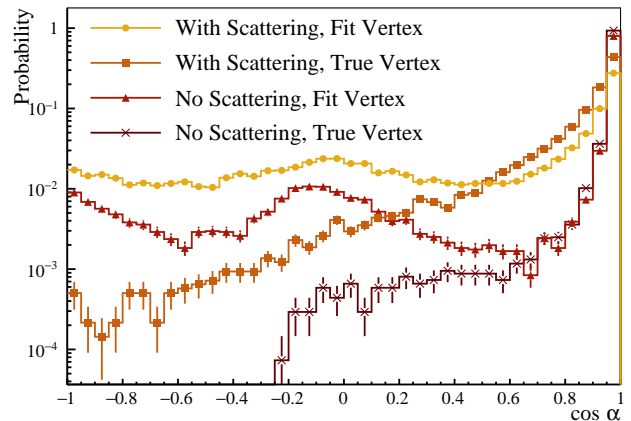


FIG. 5: Direction reconstruction of simulated 6 MeV electrons in scintillator for cases of 1) no multiple scattering and using the true vertex position (brown, cross); 2) no multiple scattering and using the fit vertex position (red, triangle); 3) multiple scatterings and using the true vertex position (orange, square); and 4) multiple scatterings and using the fit vertex position (yellow, circle).

VI. APPLICATION TO SOLAR NEUTRINOS

Direction reconstruction was applied to the solar neutrino dataset previously described, with 37 selected events containing ~ 1 expected background event. Due to the kinematics of solar neutrino elastic-scattering, the scattered electrons have additional angular spread relative to the solar direction, as indicated in Fig. 2b. Due to the selection of electrons with an energy greater than 5 MeV, this smearing is confined to one bin. The results of direction reconstruction in data are shown in Fig. 6, along with Monte Carlo (MC) predictions sampled from a nominal ^8B energy spectrum. A clear peak at $\cos \theta_{\text{Sun}} = 1$ can be seen. A likelihood ratio test in comparison with an isotropic distribution yields a p -value corresponding to 5.7σ .

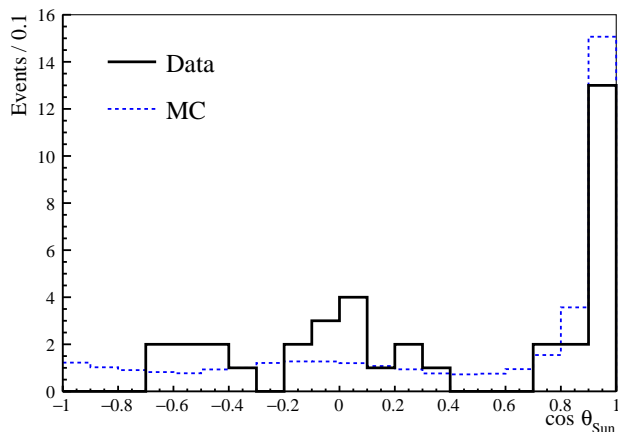


FIG. 6: Results of direction reconstruction for measured (solid) and simulated (dashed) ^8B solar neutrinos, where simulation sampled from a nominal ^8B energy spectrum.

VII. CONCLUSIONS

Data from the SNO+ experiment has been used to demonstrate event-by-event direction reconstruction of recoil electrons from solar neutrinos for the first time, exploiting the time separation of the directional Cherenkov light from the scintillation light. Remarkably, this

demonstrates the ability to achieve comparable directional information to that of water Cherenkov detectors, which has played a crucial role in numerous fundamental measurements. This new capability opens up interesting possibilities for current detectors and for the design of future instruments. Potential applications include studies of solar neutrinos, supernova neutrinos, and background discrimination for other physics. By utilizing slower scintillators, increased photocathode coverage and/or other developing technologies, this approach could be extended to lower energies, where it could also provide important background suppression (such as from ^8B solar neutrinos) in studies of phenomena such as neutrinoless double beta decay.

Capital funds for SNO+ were provided by the Canada Foundation for Innovation and matching partners: Ontario Ministry of Research, Innovation and Science, Alberta Science and Research Investments Program, Queen's University at Kingston, and the Federal Economic Development Agency for Northern Ontario. This research was supported by (Canada) the Natural Sciences and Engineering Research Council of Canada, the Canadian Institute for Advanced Research, the Ontario Early Researcher Awards; (U.S.) the Department of Energy (DOE) Office of Nuclear Physics, the National Science Foundation, and the DOE National Nuclear Security Administration through the Nuclear Science and Security Consortium; (U.K.) the Science and Technology Facilities Council and the Royal Society; (Portugal) Fundação para a Ciência e a Tecnologia (FCT-Portugal); (Germany) the Deutsche Forschungsgemeinschaft; (Mexico) DGAPA-UNAM and Consejo Nacional de Ciencia y Tecnología; and (China) the Discipline Construction Fund of Shandong University. We also thank SNOLAB and SNO+ technical staff; the Digital Research Alliance of Canada; the GridPP Collaboration and support from Rutherford Appleton Laboratory, and the Savio computational cluster at the University of California, Berkeley. Additional long-term storage was provided by the Fermilab Scientific Computing Division.

For the purposes of open access, the authors have applied a Creative Commons Attribution licence to any Author Accepted Manuscript version arising. Representations of the data relevant to the conclusions drawn here are provided within this paper.

-
- [1] M. Agostini *et al.* (Borexino Collaboration), Experimental evidence of neutrinos produced in the CNO fusion cycle in the Sun, *Nature* **587**, 577 (2020).
 - [2] K. Eguchi *et al.* (KamLAND Collaboration), First results from KamLAND: Evidence for reactor anti-neutrino disappearance, *Phys. Rev. Lett.* **90**, 021802 (2003).
 - [3] F. P. An *et al.* (Daya Bay Collaboration), Observation of electron-antineutrino disappearance at Daya Bay, *Phys. Rev. Lett.* **108**, 171803 (2012).
 - [4] J. K. Ahn *et al.* (RENO Collaboration), Observation of reactor electron antineutrinos disappearance in the reno experiment, *Phys. Rev. Lett.* **108**, 191802 (2012).
 - [5] Y. Abe *et al.* (Double Chooz Collaboration), Reactor electron antineutrino disappearance in the Double Chooz experiment, *Phys. Rev. D* **86**, 052008 (2012).
 - [6] S. Abe *et al.* (KamLAND-Zen Collaboration), First search for the majorana nature of neutrinos in the inverted mass ordering region with KamLAND-Zen, *Phys.*

- Rev. Lett. **130**, 051801 (2023).
- [7] G. Alimonti *et al.* (Borexino Collaboration), The Borexino detector at the Laboratori Nazionali del Gran Sasso, *Nucl. Instrum. Methods Phys. Res. Sect. A* **600**, 568 (2009).
- [8] H. Ozaki and A. Takeuchi (KamLAND-Zen Collaboration), Upgrade of the KamLAND-Zen mini-balloon and future prospects, *Nucl. Instrum. Methods Phys. Res. Sect. A* **958**, 162353 (2020).
- [9] V. Albanese *et al.* (SNO+ Collaboration), The SNO+ experiment, *J. Instrum.* **16**, P08059 (2021).
- [10] F. An *et al.* (JUNO Collaboration), Neutrino physics with JUNO, *J. Phys. G* **43**, 030401 (2016).
- [11] M. Askins *et al.* (Theia Collaboration), THEIA: An advanced optical neutrino detector, *Eur. Phys. J. C* **80**, 1 (2020).
- [12] J. F. Beacom *et al.*, Physics prospects of the Jinping neutrino experiment, *Chin. Phys. C* **41**, 023002 (2017).
- [13] S. D. Biller, Probing Majorana neutrinos in the regime of the normal mass hierarchy, *Phys. Rev. D* **87**, 071301 (2013).
- [14] C. Aberle, A. Elagin, H. J. Frisch, M. Wetstein, and L. Winslow, Measuring directionality in double-beta decay and neutrino interactions with kiloton-scale scintillation detectors, *J. Instrum.* **9**, P06012 (2014).
- [15] M. Li, Z. Guo, M. Yeh, Z. Wang, and S. Chen, Separation of scintillation and cherenkov lights in linear alkyl benzene, *Nucl. Instrum. Methods Phys. Res. Sect. A* **830**, 303 (2016).
- [16] Z. Guo, M. Yeh, R. Zhang, D.-W. Cao, M. Qi, Z. Wang, and S. Chen, Slow liquid scintillator candidates for MeV-scale neutrino experiments, *Astropart. Phys.* **109**, 33 (2019).
- [17] M. Yeh, S. Hans, W. Beriguete, R. Rosero, L. Hu, R. Hahn, M. Diwan, D. Jaffe, S. Kettell, and L. Littenberg, A new water-based liquid scintillator and potential applications, *Nucl. Instrum. Methods Phys. Res. Sect. A* **660**, 51 (2011).
- [18] J. Gruszko, B. Naranjo, B. Daniel, A. Elagin, D. Gooding, C. Grant, J. Ouellet, and L. Winslow, Detecting Cherenkov light from 1–2 MeV electrons in linear alkylbenzene, *J. Instrum.* **14**, P02005 (2019).
- [19] T. Kaptanoglu, M. Luo, B. Land, A. Bacon, and J. R. Klein, Spectral photon sorting for large-scale Cherenkov and scintillation detectors, *Phys. Rev. D* **101**, 072002 (2020).
- [20] T. Kaptanoglu, M. Luo, and J. Klein, Cherenkov and scintillation light separation using wavelength in LAB based liquid scintillator, *J. Instrum.* **14**, T05001 (2019).
- [21] J. Caravaca, F. B. Descamps, B. J. Land, M. Yeh, and G. D. Orebi Gann, Cherenkov and scintillation light separation in organic liquid scintillators, *Eur. Phys. J. C* **77**, 811 (2017).
- [22] B. J. Land, Z. Bagdasarian, J. Caravaca, M. Smiley, M. Yeh, and G. D. Orebi Gann, MeV-scale performance of water-based and pure liquid scintillator detectors, *Phys. Rev. D* **103**, 052004 (2021).
- [23] R. Bonventre and G. D. Orebi Gann, Sensitivity of a low threshold directional detector to CNO-cycle solar neutrinos, *Eur. Phys. J. C* **78**, 435 (2018).
- [24] T. Kaptanoglu, E. J. Callaghan, M. Yeh, and G. D. Orebi Gann, Cherenkov and scintillation separation in water-based liquid scintillator using an LAPPDTM, *Eur. Phys. J. C* **82**, 169 (2022).
- [25] J. Dunger, E. J. Leming, and S. D. Biller, Slow-fluor scintillator for low energy solar neutrinos and neutrinoless double beta decay, *Phys. Rev. D* **105**, 092006 (2022).
- [26] P. Huber *et al.*, Snowmass Neutrino Frontier Report, [arXiv:2211.08641](https://arxiv.org/abs/2211.08641).
- [27] J. R. Klein *et al.*, Future advances in photon-based neutrino detectors: A snowmass white paper, [arXiv:2203.07479](https://arxiv.org/abs/2203.07479).
- [28] E. C. for Future Accelerator Detector R&D Roadmap Process Group (CERN), The 2021 ECFA Detector Research and Development Roadmap, [10.17181/CERN.XDPL.W2EX.1](https://arxiv.org/abs/10.17181/CERN.XDPL.W2EX.1) (2021).
- [29] B. Acharya *et al.*, Fundamental symmetries, neutrons, and neutrinos (FSNN): Whitepaper for the 2023 NSAC long range plan, [arXiv:2304.03451](https://arxiv.org/abs/2304.03451).
- [30] T. Anderson *et al.*, Eos: Conceptual design for a demonstrator of hybrid optical detector technology, *J. Instrum.* **18**, P02009 (2023).
- [31] ANNIE Collaboration, ANNIE Detector R&D, SNOWMASS Letter of Interest (2021).
- [32] R. Svoboda, Status of the 30-ton Purification Demonstrator at Brookhaven, in *TAUP 2023* (University of Vienna, 2023).
- [33] C. Athanassopoulos *et al.* (LSND Collaboration), The liquid scintillator neutrino detector and LAMPF neutrino source, *Nucl. Instrum. Methods Phys. Res. Sect. A* **388**, 149 (1997).
- [34] M. H. Shaevitz (MiniBooNE Collaboration), Miniboone oscillation results and implications, *J. Phys. Conf. Ser.* **120**, 052003 (2008).
- [35] A. A. Aguilar-Arevalo *et al.* (MiniBooNE Collaboration), The MiniBooNE detector, *Nucl. Instrum. Methods Phys. Res. Sect. A* **599**, 28 (2009).
- [36] S. D. Biller, E. J. Leming, and J. L. Paton, Slow fluors for effective separation of Cherenkov light in liquid scintillators, *Nucl. Instrum. Methods Phys. Res. Sect. A* **972**, 164106 (2020).
- [37] M. Agostini *et al.* (Borexino Collaboration), First directional measurement of sub-MeV solar neutrinos with Borexino, *Phys. Rev. Lett.* **128**, 0981803 (2022).
- [38] D. Basilico *et al.* (Borexino Collaboration), Final results of Borexino on CNO solar neutrinos, *Phys. Rev. D* **108**, 102005 (2023).
- [39] M. Anderson *et al.* (SNO+ Collaboration), Development, characterisation, and deployment of the SNO+ liquid scintillator, *J. Instrum.* **16**, P05009 (2021).
- [40] S. Andringa *et al.* (SNO+ Collaboration), Current status and future prospects of the SNO+ experiment, *Adv. High Energy Phys.* , 6194250 (2016).
- [41] E. Vitagliano, I. Tamborra, and G. Raffelt, Grand unified neutrino spectrum at earth: Sources and spectral components, *Rev. Mod. Phys.* **92**, 045006 (2020).